



Characterization, molecular structures and fluorescent properties of Pd(II) and Ni(II) complexes with 1-benzyl-2-methylimidazole

J.G. Małecki*, A. Maroń

Department of Crystallography, Institute of Chemistry, University of Silesia, 9th Szkolna St., 40-006 Katowice, Poland

ARTICLE INFO

Article history:

Received 27 July 2012

Accepted 27 November 2012

Available online 6 December 2012

Keywords:

Palladium(II) and nickel(II)
1-Benzyl-2-methylimidazole
X-ray structure
Electronic structure
DFT calculations
Fluorescence

ABSTRACT

The paper presents a combined experimental and computational study of Pd(II) and Ni(II) complexes containing chloride, thiocyanate and 1-benzyl-2-methylimidazole ligands. The complexes were studied by IR, ¹H NMR, UV–Vis spectroscopy and X-ray crystallography. Electronic structures of the complexes have been calculated using the density functional theory (DFT) method. Spin-allowed electronic transitions have been calculated using the time-dependent DFT method and the UV–Vis spectrum has been discussed on this basis. Luminescence properties of the complexes have been examined.

© 2012 Elsevier Ltd. All rights reserved.

1. Introduction

Palladium(II) complexes currently attract a considerable interest because of their potentially beneficial pharmacological properties. Palladium complexes with aromatic N-containing ligands, e.g. derivatives of pyridine, quinoline, pyrazole and 1,10-phenanthroline, have shown very promising antitumor characteristics [1–4]. Some of these complexes, especially the *trans* analogs with nonplanar heterocyclic amine ligands, have been found to overcome multifactorial cisplatin resistance in human ovarian cell lines [5,6]. On the other hand, Pd(II) complexes have been widely explored due to their catalytic efficiency, e.g. for various carbon–carbon and carbon–nitrogen bond-forming reactions [7–11]. Whilst most studies of palladium have concentrated on the reactivity of its complexes, little information about their electronic structures has been obtained. On the other hand four-coordinate palladium(II) complexes with square-planar geometry and various N-heteroaromatic ligands are one large class of useful building blocks for producing interesting molecular structures by combination of coordination chemistry and hydrogen bonding [12].

Complexes with N-heteroaromatic ligands and such metals as ruthenium(II), osmium(II) and rhenium(I) are by far the most studied due to their luminescent properties. In contrast d⁸ metal complexes have been much less studied. The luminescent properties of palladium(II) complexes strongly depend on their electronic structure. For this reason, study of the electronic structures of such

complexes is valuable as a means to the prediction of their properties [13–16].

Here is reported an experimental and quantum chemical study of two cationic palladium(II) complexes with pyrazole derivative ligands. The quantum chemical study included a characterization of the molecular and electronic structures of the complex by analysis of optimized molecular geometry, electronic populations by using the natural bond orbitals scheme. The latter was used to identify the nature of the interactions between the ligands and the central ion. The calculated density of states showed the interactions and influences the orbital composition in the frontier electronic structure. The time dependent density functional theory (TD-DFT) was finally used to calculate the electronic absorption spectrum. Based on a molecular orbital scheme, these results allowed the interpretation of the UV–Vis spectrum obtained at an experimental level.

2. Experimental

All reagents used for the synthesis of the complexes are commercially available and have been used without further purification. All operations were carried out in air.

2.1. Synthesis of [Pd(X)₂(PhCH₂ImCH₃)₂] where X = Cl; SCN complexes

1-Benzyl-2-methylimidazole (0.32 cm³, ~2 mmol) was dissolved in acetonitrile (10 cm³) and then slowly added to warm solution of PdCl₂ (0.18 g, 1 mmol) (in the synthesis of thiocyanate complex the NH₄SCN (0.15 g, 2 mmol) was added) in acetonitrile

* Corresponding author.

E-mail address: gmalecki@us.edu.pl (J.G. Małecki).

(30 cm³). The mixture was refluxed for about 2 h and after the time the reaction solution was filtered and yellow single crystals were obtained by slow evaporation of the solvent. Yield: 88% for chloride complex (**1**) and 92% for thiocyanate analog (**2**).

(**1**): IR (KBr): 3155 ν_{ArH} ; 2927 ν_{CH} ; 1543 ν_{CN} , 1497 $\nu_{\text{C=C}}$; 1454, 1351 $\delta_{\text{(C-CH in the plane)}}$; 1274, 1155 $\delta_{\text{(N-CH in the plane)}}$; 1067 $\delta_{\text{(CH}_3)}$; 750, 695 $\delta_{\text{(Im ring)}}$.

¹H NMR (400 MHz, CDCl₃) δ 7.43–7.26 (m, Ph), 7.17 (d, $J = 1.8$ Hz, Im), 7.13–7.06 (m, Ph), 6.74 (d, $J = 1.8$ Hz, Im), 5.03 (s, CH₂), 2.92 (s, CH₃).

UV–Vis (acetonitrile, λ (nm)): 401.5, 276.1, 228.4, 211.5.

(**2**): IR (KBr): 3152 ν_{ArH} ; 2927 ν_{CH} ; 2117 $\nu_{\text{CN from SCN}}$; 1550 ν_{CN} , 1503 $\nu_{\text{C=C}}$; 1448, 1354 $\delta_{\text{(C-CH in the plane)}}$; 1281, 1166 $\delta_{\text{(N-CH in the plane)}}$; 1077 $\delta_{\text{(CH}_3)}$; 723 $\nu_{\text{SC from SCN}}$.

¹H NMR (400 MHz, CDCl₃) δ 7.47–6.98 (m, Ph; Im), 6.76 (d, $J = 1.8$ Hz, Im), 5.09 (d, $J = 13.2$ Hz, CH₂), 2.92 (s, CH₃).

UV–Vis (acetonitrile, λ (nm) (log ϵ): 400.1, 325.6, 264.6, 232.5, 212.7.

2.2. Synthesis of [Ni(NCS)₂(PhCH₂ImCH₃)₄].CH₃OH

The 1-benzyl-2-methylimidazole (0.64 cm³, ~4 mmol) was added to the solution of NiCl₂·6H₂O (0.24 g, ~1 mmol) and NH₄SCN (0.15 g, 2 mmol) in methanol (50 cm³). The mixture was refluxed for about 2 h and after the time the reaction solution was filtered and blue single crystals were obtained by slow evaporation of the solvent.

(**3**): IR (KBr): 3119, 3030 ν_{ArH} ; 2954 ν_{CH} ; 2094 $\nu_{\text{CN from SCN}}$; 1537 ν_{CN} , 1495 $\nu_{\text{C=C}}$; 1451, 1415 1351 $\delta_{\text{(C-CH in the plane)}}$; 1280, 1140 $\delta_{\text{(N-CH in the plane)}}$; 988 $\delta_{\text{(CH}_3)}$; 726 $\nu_{\text{SC from SCN}}$.

UV–Vis (methanol, λ (nm)): 1069.7, 647.8, 414.5, 267.6, 264.3, 258.2, 252.2, 247.2, 211.4.

2.3. Physical measurements

Infrared spectra were recorded on a Nicolet Magna 560 spectrophotometer in the spectral range of 4000–400 cm⁻¹ using KBr pellets. Electronic spectra were measured on a Lab Alliance UV–Vis 8500 spectrophotometer in the range of 600–180 nm in methanolic solution. ¹H NMR spectrum was obtained at room temperature in DMSO-d₆ using a Bruker 400 MHz spectrometer. Luminescence measurements were made in ethanolic solutions on an F-2500 FL spectrophotometer at room temperature.

Quantum yields of fluorescence were calculated using follow equation: $\Phi_s = \Phi_{\text{std}} \frac{\text{Grad}_s \eta_s^2}{\text{Grad}_{\text{std}} \eta_{\text{std}}^2}$, where Φ_s – quantum yield of unknown sample; Φ_{std} – quantum yield of naphthalene as reference at 313 nm equal to 0.21 [17]; Grad_s and Grad_{std} are the gradients from the plot of integrated fluorescence intensity versus the solutions absorbance at the excitation wavelength and η_s and η_{std} are the refractive indices of the solvents. Samples were prepared with absorbance less than 0.1 at excitation wavelengths in order to minimize re-absorption effects and avoid inner-filter effects, which may perturb the quantum yields values. Solvent (ethanol) using in the measurements was spectroscopic grade and checked for background fluorescence.

2.4. Computational methods

Calculations were carried out using GAUSSIAN09 [18] program. Molecular geometry of the singlet ground state of complex was fully optimized in the gas phase at the B3LYP/DZVP level of theory [19,20]. The frequency calculation was carried out, verifying whether the optimized molecular structure corresponds to energy minimum, thus only positive frequencies were expected. The DZVP basis set [21] was used to describe the palladium atom and the basis set used for the lighter atoms (C, N, O, H, S) was 6-31G with a set

of “d” and “p” polarization functions. The TD-DFT (time dependent density functional theory) method [22] was employed to calculate the electronic absorption spectrum of the complex in the solvent PCM (Polarizable Continuum Model) model. In this work, 80 singlet excited states were calculated as vertical transitions for the complex. A natural bond orbital (NBO) analysis was also made for the complex using the NBO 5.0 package [23] included in GAUSSIAN09. Natural bond orbitals are orbitals localized on one or two atomic centers, that describe molecular bonding in a manner similar to a Lewis electron pair structure, and they correspond to an orthonormal set of localized orbitals of maximum occupancy. NBO analysis provides the contribution of atomic orbitals (s, p, d) to the NBO σ and π hybrid orbitals for bonded atom pairs. In this scheme, three NBO hybrid orbitals are defined, bonding orbital (BD), lone pair (LP), and core (CR), which were analyzed on the atoms directly bonded to or presenting some kind of interaction with the palladium atom. The contribution of a group (ligands, central ion) into a molecular orbital was calculated using Mulliken population analysis. GAUSSIAN2.2 [24] was used to calculate group contributions to the molecular orbitals and to prepare the partial density of states (DOS) spectra. The DOS spectra were created by convoluting the molecular orbital information with Gaussian curves of unit height and FWHM (full width at half maximum) of 0.3 eV.

2.5. Crystal structures determination and refinement

X-ray intensity data were collected with graphite monochromated Mo K α radiation at temperature of 295.0(2) K, with ω scan mode. Lorentz, polarization and empirical absorption correction using spherical harmonics implemented in SCALE3 ABSPACK scaling algorithm [CrysAlis RED, Oxford Diffraction Ltd., Version 1.171.29.2] were applied. The structure was solved by Patterson method and subsequently completed by difference Fourier recycling. All the non-hydrogen atoms were refined anisotropically using full-matrix, least-squares technique. All the hydrogen atoms were found from difference Fourier synthesis after four cycles of anisotropic refinement, and refined as riding on the parent carbon atom with individual isotropic temperature factor equal 1.2 times the value of equivalent temperature factor of the parent atom. The OLEX2 [25] and SHELXS97, SHELXL97 [26] programs were used for all the calculations.

3. Results and discussion

3.1. Spectroscopic characterization and molecular structure of the complexes

The complexes were synthesized in a simple reaction between palladium(II) or nickel(II) dichloride, ammonium thiocyanate and 1-benzyl-2-methylimidazole in acetonitrile in the case of palladium complexes (**1**) and (**2**) or methanol in (**3**) solutions. The reactions have been carried out using molar ratio 1:2:2 – palladium complexes and 1:4:2 nickel(II) complex. The IR spectra of the complexes present imidazole C=N and C=C stretches bands with maxima at 1550–1537 and 1503–1495 cm⁻¹ ranges. The ν_{CN} and ν_{CS} frequencies of thiocyanato ligands present maxima at 2117 and 723 cm⁻¹ in the case of palladium complex (**2**) and 2094, 726 cm⁻¹ in nickel(II) complex (**3**). The strong band above 2100 cm⁻¹ is characteristic for S-bonded end-on NCS⁻ coordination and for N-bonded complexes, generally the C–N stretching band is in a lower region around 2050 cm⁻¹. However, the frequencies of the bands are sensitive to other factors like coexisting ligands and the structure of the compounds were determined using X-ray analysis. While the M–S–C angles of S-bonded

Table 1
Crystal data and structures refinement details of [PdCl₂(PhCHImCH)₂] (**1**), [Pd(SCN)₂(PhCHImCH)₂] (**2**) and [Ni(NCS)₂(PhCHImCH)₄].CH₃OH (**3**) complexes.

Empirical formula	C ₂₂ H ₂₄ Cl ₂ N ₄ Pd (1)	C ₂₄ H ₂₄ N ₆ PdS ₂ (2)	C ₄₆ H ₄₈ N ₁₀ NiS ₂ , CH ₄ O (3)
Formula weight	521.75	567.01	895.84
<i>T</i> (K)	295.0(2)	295.0(2)	295.0(2)
Crystal system	triclinic	monoclinic	triclinic
Space group	<i>P</i> $\bar{1}$	<i>C</i> 2/ <i>c</i>	<i>P</i> $\bar{1}$
<i>Unit cell dimensions</i>			
<i>a</i> (Å)	7.7343(6)	31.611(2)	9.8141(4)
<i>b</i> (Å)	8.1076(5)	6.1127(4)	12.5425(6)
<i>c</i> (Å)	9.7896(6)	12.7977(9)	19.7021(9)
α (°)	100.719(5)	90	82.035(4)
β (°)	94.589(6)	92.346(7)	85.048(3)
γ (°)	113.906(6)	90	83.202(4)
<i>V</i> (Å ³)	543.10(6)	2470.9(3)	2378.86(19)
<i>Z</i>	1	4	2
<i>D</i> _{calc} (Mg/m ³)	1.595	1.524	1.251
Absorption coefficient (mm ⁻¹)	1.116	0.944	0.541
<i>F</i> (000)	264	1152	944
Crystal dimensions (mm)	0.34 × 0.20 × 0.04	0.17 × 0.09 × 0.04	0.24 × 0.05 × 0.04
θ (°)	3.65–25.05	3.39–25.05	3.35–25.05
Index ranges	−9 ≤ <i>h</i> ≤ 9, −9 ≤ <i>k</i> ≤ 9, −11 ≤ <i>l</i> ≤ 11	−37 ≤ <i>h</i> ≤ 36, −7 ≤ <i>k</i> ≤ 7, −15 ≤ <i>l</i> ≤ 15	−11 ≤ <i>h</i> ≤ 11, −14 ≤ <i>k</i> ≤ 14, −23 ≤ <i>l</i> ≤ 23
Reflections collected	4094	8794	17804
Independent reflections (<i>R</i> _{int})	1926 (0.0263)	2181 (0.0336)	8397 (0.0360)
Data/restraints/parameters	1926/0/134	2181/0/152	8397/0/567
Goodness-of-fit (GOF) on <i>F</i> ²	1.036	1.063	0.980
Final <i>R</i> indices [<i>I</i> > 2σ(<i>I</i>)]	<i>R</i> ₁ = 0.0238, <i>wR</i> ₂ = 0.0572	<i>R</i> ₁ = 0.0269, <i>wR</i> ₂ = 0.0624	<i>R</i> ₁ = 0.0476, <i>wR</i> ₂ = 0.1007
<i>R</i> indices (all data)	<i>R</i> ₁ = 0.0251, <i>wR</i> ₂ = 0.0578	<i>R</i> ₁ = 0.0390, <i>wR</i> ₂ = 0.0670	<i>R</i> ₁ = 0.0875, <i>wR</i> ₂ = 0.1122
Largest difference peak and hole	0.362 and −0.376	0.430 and −0.306	0.289 and −0.187

thiocyanato ligand in complexes are bent around 110°, the M–N–C angles of *N*-bonded isothiocyanato ligands are close to linear.

The ¹H NMR spectra of (**1**) and (**2**) complexes show characteristic signals of imidazole derivative hydrogens. The signals at 6.74, 5.03 and 2.92 ppm are attributed to C(2)H, CH₂ and CH₃ protons of 1-benzyl-2-methylimidazole, respectively. The proton NMR spectrum for nickel(II) complex was not measured due to paramagnetic d⁸ configuration of nickel central ion in octahedral ligand field.

The complexes crystallize in triclinic *P* $\bar{1}$ (**1**) and (**3**) and monoclinic *C*2/*c* complex (**2**) space groups. Moreover nickel(II) complex (**3**) crystallizes in a form solvated by one methanol molecule. Details concerning crystal data and refinement are gathered in Table 1. Fig. 1 presents molecular structures, and selected bond distances and angles are presented in Table 2. The slightly increases values of *R*₁ and *wR*₂ indices equal to 0.0476 and 0.1122 in the case of complex (**3**) are from the quality of measured crystal. In the structure of this complex the sulfur S(2) atom is disordered what on one hand is resulted from the quality of the crystal and on the other hand is connected with the short contact interactions between S(2)/(2A) and C(27)–H(27A), C(43)–H(43) atoms of 1-benzyl-2-methylimidazole ligands generated by symmetry operations. The S(2A)···H(43)–C(43)[*x*, −1 + *y*, *z*] and S(2A)···H(27A)–C(27)[2 − *x*; 1 − *y*; 2 − *z*], S(2)···H(27A)–C(27)[2 − *x*; 1 − *y*; 2 − *z*] distances are 2.946 and 2.876, 2.832 Å respectively. From the second reason the dynamical disorder could be considered and determination of the structure in the low temperature should eliminate this factor. Palladium(II) atoms in the complexes (**1**) and (**2**) have square planar environments with the 1-benzyl-2-methylimidazole ligands bonded to the metal centre through the imidazole nitrogen atoms and thiocyanate by sulfur (complex **2**). The halide and imidazole derivative ligands in complexes (**1**) and (**2**) are mutually *trans* disposed. The structure of octahedral complex (**3**) with 1-benzyl-2-methylimidazole ligands in the equatorial plane and mutually *trans* NCS[−] ligand may be described by D_{4h} Schoenflies symbol and the palladium(II) complexes (**1**) and (**2**) have D_{2h} symmetry.

In the molecular structure of nickel(II) complex (**3**) the thiocyanate ligands are bonded to central ion by nitrogen donor atoms occur the isothiocyanate form. The differences in the bonding of thiocyanate ligands in the palladium and nickel complexes are visible in the angles between central ions and pseudohalide ligands equal to 106.35(10)° in (**2**) and 159.0(2)°, 163.3(3)° in complex (**3**) adequate to S- and N-bonding mode of NCS[−]. The Pd–N distances in both complexes are very close and by about 0.1 Å shorter than Ni–N_(lm) distances. The Pd(1)–Cl(1) bond length fall within a usual range (2.298–2.354 Å) reported for four-coordinate palladium(II) complexes [27]. The Pd(1)–S(CN) and Ni(1)–N(CS) bonds lengths are also normal. Square planar environments of palladium as well as octahedral geometry in complex (**3**) are distorted and the deviation from the expected 90° bond angles comes from the angles between thiocyanato and imidazole derivative ligands. The deviations of N_(lm)–M–S(N) angles from the right angle do not exceed 3°.

In the crystal structures of the (**1**) and (**3**) complexes several weak inter- and intramolecular hydrogen bonds exist [28] given in Table 3. The packing of molecules of (**1**) is presented on the Fig. 2 and as one can see the complex molecules form layers along *a* axis linking by C(4)–H(4A)···Cl(1) hydrogen bond. In the structure of thiocyanate complex (**2**) an infinite one-dimensional chain along *b* axis is created by interaction between sulfur atoms generated by 1 − *x*, *y*, −1/2 − *z* symmetry. In the case of nickel(II) complex (**3**) except the hydrogen bonds the stacking contacts as presented on Fig. 2 are visible. The C–H···π distances between imidazole C(35)[−1 + *x*; *y*; *z*]···H(16B)C(16), C(24)–H(24)[1 + *x*; *y*; *z*]···C(40) and parallel-dispaced π-stacking between phenyl rings C(7)–C(11)···C(7)–C(11)[2 − *x*, −*y*, 1 − *z*] are 3.224, 2.818 and 3.380 Å respectively.

3.2. Electronic structure

To obtain an insight in electronic structures and bonding properties of the complex, calculations using the density functional

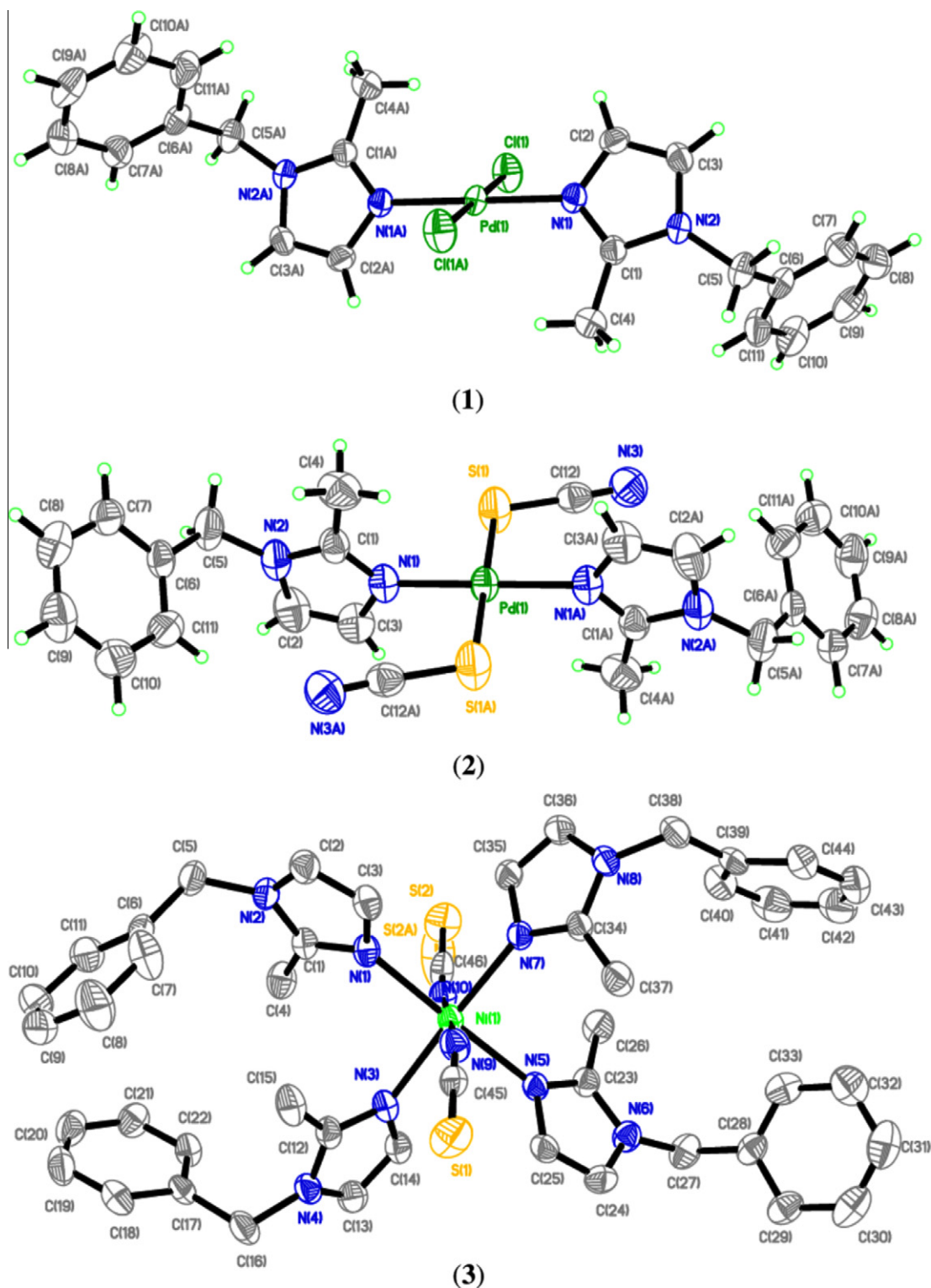


Fig. 1. Molecular structures of $[\text{PdCl}_2(\text{PhCHImCH})_2]$ (1), $[\text{Pd}(\text{SCN})_2(\text{PhCHImCH})_2]$ (2) and $[\text{Ni}(\text{NCS})_2(\text{PhCHImCH})_4] \cdot \text{CH}_3\text{OH}$ (3) complexes with anisotropic displacement parameters shown at the 50% probability level. On the structure of complex (3) the hydrogen atoms and solvent molecule were omitted for clarity.

theory (DFT) method with the B3LYP functional of GAUSSIAN09 were carried out. Before the calculations, their geometry was optimized in singlet states using the DFT method with the B3LYP functional. In general, the predicted bond lengths and angles are in good agreement with the values based on the X-ray crystal structure data, and the general trends observed in the experimental data are well reproduced in the calculations as one can see from the

data given in Table 2. Vibrational harmonic frequency analyses of the optimized geometries were utilized to ensure that it is true local minimum having no imaginary frequencies. From the data collected in this table, it may be seen that the bond lengths are maximally elongated by $\sim 0.1 \text{ \AA}$ in the calculated gas phase structures, while the bond angles changed maximally by 2° except the Ni–NCS bonds which the negligence of intermolecular interactions

Table 2

Selected bond lengths (Å) and angles (°) with the optimized geometry values for [PdCl₂(PhCHImCH)₂] (1), [Pd(SCN)₂(PhCHImCH)₂] (2) and [Ni(NCS)₂(PhCHImCH)₄]-CH₃OH (3) complexes.

	(1)		(2)	
	Exp.	Calc.	Exp.	Calc.
	Exp.	Calc.		
<i>Bond lengths (Å)</i>				
Pd(1)–Cl(1)	2.3011(6)	2.38		
Pd(1)–N(1)	2.0202(17)	2.08	2.023(2)	2.08
Pd(1)–S(1)			2.3202(8)	2.42
S(1)–C(12)			1.656(3)	1.69
N(3)–C(12)			1.144(4)	1.17
<i>Angles (°)</i>				
N(1)–Pd(1)–Cl(1)	89.40(5)	89.26		
N(1)–Pd(1)–S(1)			86.05(7)	85.50
Pd(1)–S(1)–C(12)			106.35(10)	105.80
N(3)–C(12)–S(1)			176.2(3)	178.17
	(3)			
	Exp.	Calc.		
<i>Bond lengths (Å)</i>				
Ni(1)–N(1)	2.133(2)	2.16		
Ni(1)–N(3)	2.135(2)	2.17		
Ni(1)–N(5)	2.1339(19)	2.17		
Ni(1)–N(7)	2.126(2)	2.16		
Ni(1)–N(9)	2.077(3)	2.06		
Ni(1)–N(10)	2.073(3)	2.05		
S(1)–C(45)	1.633(3)	1.69		
S(2)–C(46)	1.663(8)	1.69		
N(9)–C(45)	1.147(3)	1.19		
N(10)–C(46)	1.137(3)	1.19		
<i>Angles (°)</i>				
N(10)–Ni(1)–N(9)	177.71(8)	178.8		
N(1)–Ni(1)–N(7)	89.88(9)	90.8		
N(9)–Ni(1)–N(7)	91.45(9)	92.7		
N(10)–Ni(1)–N(1)	88.94(8)	88.6		
N(9)–Ni(1)–N(1)	89.24(8)	90.2		
N(7)–Ni(1)–N(1)	88.34(8)	88.5		
N(10)–Ni(1)–N(5)	92.58(8)	92.0		
N(9)–Ni(1)–N(5)	89.28(8)	89.2		
N(7)–Ni(1)–N(5)	89.98(8)	88.5		
N(1)–Ni(1)–N(5)	177.73(10)	177.7		
N(10)–Ni(1)–N(3)	89.74(9)	89.9		
N(9)–Ni(1)–N(3)	89.00(9)	89.1		
N(7)–Ni(1)–N(3)	177.67(8)	177.7		
N(1)–Ni(1)–N(3)	93.95(8)	92.7		
N(5)–Ni(1)–N(3)	87.74(8)	88.1		
Ni(1)–N(9)–C(45)	159.0(2)	170.2		
Ni(1)–N(10)–C(46)	163.3(3)	178.1		
N(9)–C(45)–S(1)	178.7(3)	179.9		
N(10)–C(46)–S(2)	162.6(13)	179.2		
S(2)[S(2A)]	[169.6(4)]			

Table 3

Hydrogen bonds for [PdCl₂(PhCHImCH)₂] (1) and [Ni(NCS)₂(PhCHImCH)₄]-CH₃OH (3) complexes (Å and °).

D–H...A	d(D–H)	d(H...A)	d(D...A)	<(DHA)
(1)				
C(4)–H(4A)...Cl(1) #1	0.96	2.80	3.545(3)	135
(3)				
C(4)–H(4A)...N(10)	0.96	2.61	3.311(3)	130
C(26)–H(26C)...N(10)	0.96	2.60	3.229(3)	123
C(37)–H(37C)...N(9)	0.96	2.54	3.264(4)	132
C(40)–H(40)...N(8)	0.93	2.57	2.882(4)	100

Symmetry transformations used to generate equivalent atoms: #1 1 – x, 2 – y, –z.

for the gas phase caused significant differences between experimental and calculated values.

The formal charges of palladium and nickel central ions are +2 in the complexes but the calculated charges, obtained from natural

population analyses, are 0.44, 0.29 form (1), (2) and 1.55 form complex (3) respectively. This is a result of charge donation from the ligands to the metal center and as one can see the charge flows are much greater in the case of square planar palladium complexes than octahedral nickel(II) complex (3). These differences relate both to the number of imidazole derivative ligands in the coordination spheres and the difference between chloride and thiocyanate ligands. M–N_(lm) interactions have Coulomb-type character, which are visible in the calculated Wiberg bond indices with values considerably lower than one, 0.4, 0.2 in complexes (1), (2) and 0.1 in complex (3). The chloride and thiocyanate ligands show also non-covalent bonding with palladium and nickel with Wiberg indices 0.6 and 0.2 respectively.

Analysis of the frontier molecular orbitals is useful for understanding the spectroscopic properties, such as electronic absorption and emission spectra of organometallic complexes. The overlap partial densities of states (DOS) in terms of Mulliken population analysis were calculated using the GAUSSIAN program. As one can see from the Fig. 3 the interaction of isothiocyanate ligands with nickel(II) is weaker compared with palladium(II) complex (2). Moreover interaction of chloride ligands with Pd(II) in complex (1) is also stronger than between NCS[–] and Ni(II).

Fig. 4 presents the simplified molecular orbital diagrams for palladium complexes (1) and (2). The splitting of d palladium orbitals is specific to square planar D_{4h} symmetry of the complexes. The e_g, a_{1g}, b_{2g} and b_{1g} terms consist mainly of the palladium d orbitals with some admixture of halide ligand orbitals. The imidazole derivative ligands play role in HOMO – 4 (d_{xz}) and LUMO orbitals. In the thiocyanate complex (2) an increase in energy of the HOMO is visible and the differences in energies between b_{2g} (π_{xy}^{*}) and b_{1g} (σ_{x²–y²}^{*}) levels equals to 3.73 and 3.11 eV respectively; HOMO–LUMO gap in nickel(II) complex (3) is higher with value equal to 4.04 eV.

3.3. Absorption and emission electronic spectra

UV–Vis spectra of the palladium(II) complexes exhibit bands with maxima at 401.5, 276.1, 228.4, 211.5 nm and 400.1, 325.6, 264.6, 232.5, 212.7 nm. The nature of the electronic transitions has been analyzed using time-dependent DFT (TDDFT) based on the optimized singlet state geometry. The electronic transitions were calculated by use of the long range corrected version of the B3LYP functional – CAM-B3LYP which employs the Coulomb-attenuating method. This functional provides a better estimation of excitation energies and oscillators strengths, especially for transitions with charge-transfer character. In Table 4, several calculated electronic transitions and their assignments to the experimental absorption bands are gathered. The assignment of the calculated orbital excitations to the experimental bands was based on an overview of the composition and relative energy to the orbitals HOMO and LUMO involved in the electronic transitions.

As it may be seen from the data, *ligand-to-metal charge transfer* transitions are dominant in the electronic spectrum of the chloride complex (1). However in the spectrum of the complex charge transfer transitions from imidazole derivative ligands to b_{1g} term (π_{lm} → d_{x²–y²}) play significant role in the energy range up to 236 nm. The transition between a_{1g} and b_{1g} terms is calculated only at lowest energy band (390.1 nm). The *metal-to-ligand charge transfer* transitions were calculated at the energy close to 220 nm and the highest experimental band is attributed to *ligand-to-ligand charge transfer* processes. In case of the spectrum of thiocyanate complex (2) the transitions between terms result from splitting, in D_{2h} ligand field, palladium 4d orbitals were calculated in the whole spectrum with admixture of LMCT transitions (π_{L/SCN} → b_{1g}). The difference in the character of the spectra refers to luminescence property of the complexes.

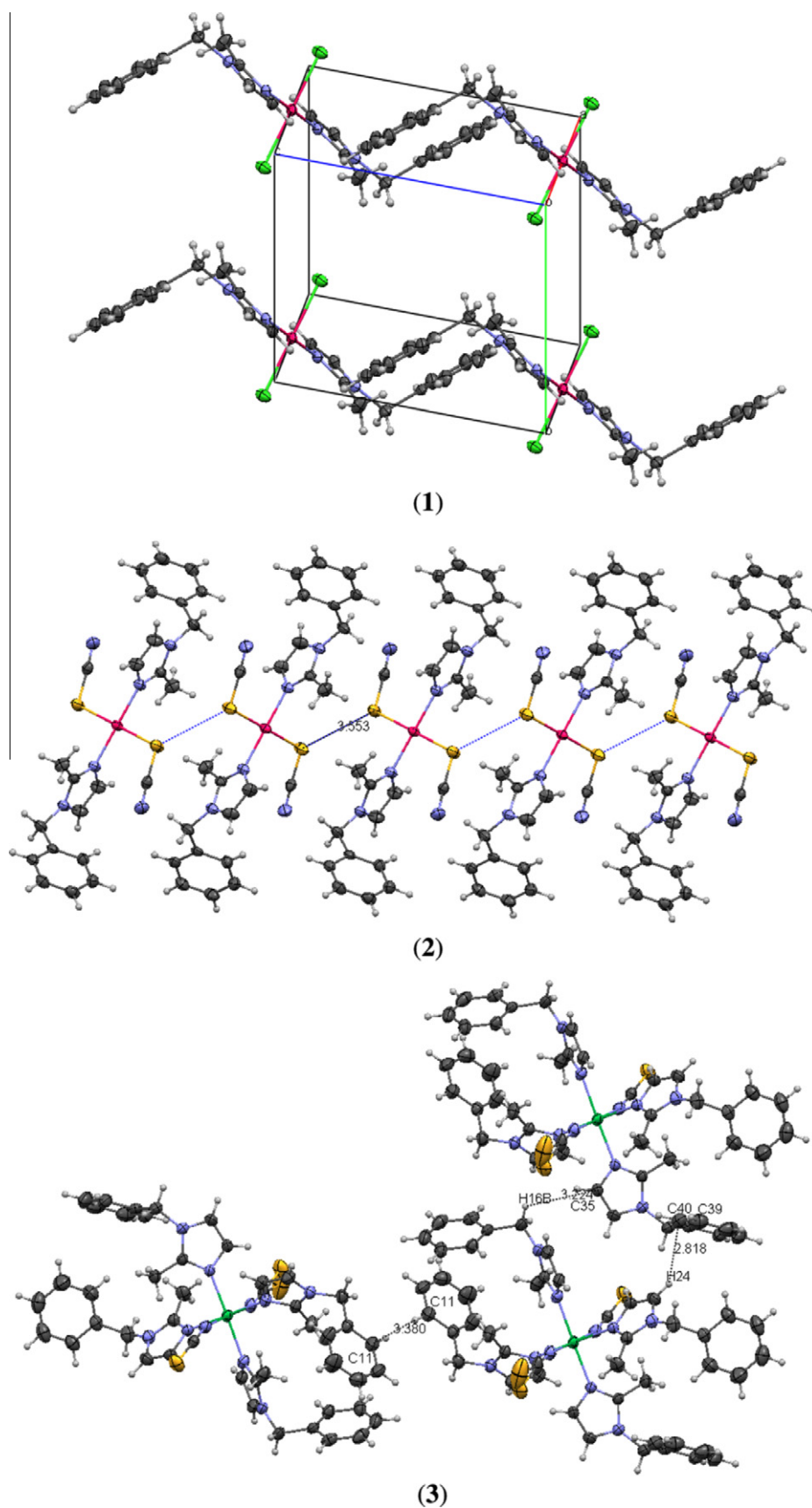


Fig. 2. Crystal packing and contacts in the crystal structures of the $[\text{PdCl}_2(\text{PhCHImCH})_2]$ (1), $[\text{Pd}(\text{SCN})_2(\text{PhCHImCH})_2]$ (2) and $[\text{Ni}(\text{NCS})_2(\text{PhCHImCH})_4]$ (3) complexes.

The lowest state of the nickel(II) ion is ^3F term, which splits into $^3\text{A}_{2g}$, $^3\text{T}_{2g}$ and $^3\text{T}_{1g}$ terms in the field with O_h symmetry and $^3\text{B}_{1g}$,

$^3\text{B}_{2g}/^3\text{E}_g$ and $^3\text{A}_{2g}/^3\text{E}_g$ in the D_{4h} symmetry. The levels are then further split by spin-orbit coupling but this coupling is small that can

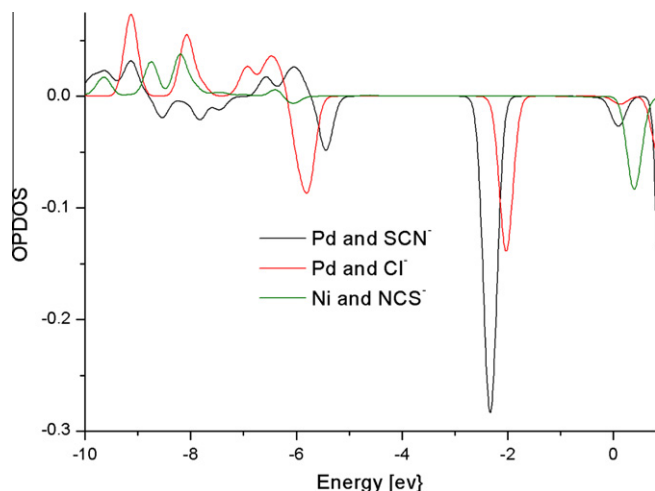


Fig. 3. The overlap partial density-of-states diagrams.

be neglected. As a consequence, the first and second spin allowed transition bands observed on the UV–Vis spectrum (1069.7, 647.8 nm) of complex **(3)** are assigned to ${}^3B_{2g}({}^3E_g({}^3F)) \rightarrow {}^3B_{1g}({}^3F)$ and ${}^3A_{2g}({}^3E_g({}^3F)) \rightarrow {}^3B_{1g}({}^3F)$, respectively. The third absorption band (414.5 nm) results from a spin allowed transition ${}^3A_{2g}({}^3E_g({}^3P)) \rightarrow {}^3B_{1g}({}^3F)$. The value of the ligand field parameter $10Dq$ of the complex calculated on the basis of electronic bands positions is equal to 9348 cm^{-1} and the Racah parameter B is equal to 1048 cm^{-1} . In consequence the nephelauxetic parameter close to one confirms Coulomb-type character of nickel(II)–ligands interactions in the complex.

Emission characteristic of the complexes have been prepared in optically diluted ethanolic solutions at room temperature. The measurement of quantum yields have been examined by comparative method using naphthalene in ethanol as a standard ($\Phi_{ST} = 0.21$). The solutions of the complexes were excited in the range between 250 and 500 nm and the fluorescence with maxima at 491, 385 and 388 nm by the excitations at 340, 303 and 311 nm

for complexes **(1)**, **(2)** and **(3)** respectively, were observed. Fig. 5 presents the excitation and fluorescence spectra. The red shifts of the emission maxima are typical to 3d and 4d metal(II) complexes and the emissions originating from the charge transfer states, derived from the excitations involving a $d_{\pi} \rightarrow \pi_{\text{ligand}}$ transitions. The quantum efficiencies are equal to 0.003 for complex **(1)**, and 0.011 for **(2)** and 0.131 for **(3)** and as can be seen thiocyanate ligands considerably increase the luminescence. Moreover the quantum efficiency of palladium complex **(3)** is ten times bigger than $[\text{Ni}(\text{NCS})_2(\text{PhCHImCH})_4] \cdot \text{CH}_3\text{OH}$ **(3)**.

In the electronic spectrum of $[\text{Pd}(\text{SCN})_2(\text{PhCHImCH})_2]$ **(2)** the $e_g/\pi_{L/\text{SCN}} \rightarrow d_{x^2-y^2}/\pi_{\text{ImCH}}^*$ (b_{1g}) transitions (MLCT character) were calculated in the energy range close to excitation wavelength. Similarly, MLCT transitions about 320 nm were calculated for complex **(3)** but with large admixture of LLCT ($\pi_{\text{Im}} \rightarrow \pi_{\text{Im}}^*$) and thus the fluorescence has less intensity and efficiency. In the case of chloride complex **(1)** the LMCT ($\pi_{\text{Im}} \rightarrow d_{x^2-y^2}$) transitions predominate that explain its weak fluorescence.

Summarizing, the new palladium(II) and nickel(II) complex with 1-benzyl-2-methylimidazole ligand have been synthesized. The molecular structures of the complexes are determined by X-ray, and spectroscopic properties as infrared, ${}^1\text{H}$ NMR, UV–Vis spectra were studied. Based on the crystal structures, computational studies were carried out in order to determine their electronic structures. Electronic spectra were calculated using of TD-DFT method and character of transitions was commented in connection with structure of molecular orbitals. Emission properties of the complexes have been examined. Based on the electronic structures of the complexes showed the contributions of ligands in terms resulted from splitting of palladium or nickel d orbitals in the complexes the emission originating from the lowest energy metal to ligand charge transfer (MLCT) state, derived from the excitation involving $d_{\pi} \rightarrow \pi_{\text{ligand}}$ transitions. In the UV–Vis spectrum of chloride complex **(1)** these kind of transitions play role at the higher energies where are covered by LLCT transitions ($\pi_{\text{Im}} \rightarrow \pi_{\text{Im}}^*$). The ligand-to-ligand charge transfer transitions occurred at the excitation energy of nickel(II) complex **(3)** are also responsible for lower, compared with $[\text{Pd}(\text{SCN})_2(\text{PhCHImCH})_2]$, fluorescence efficiency

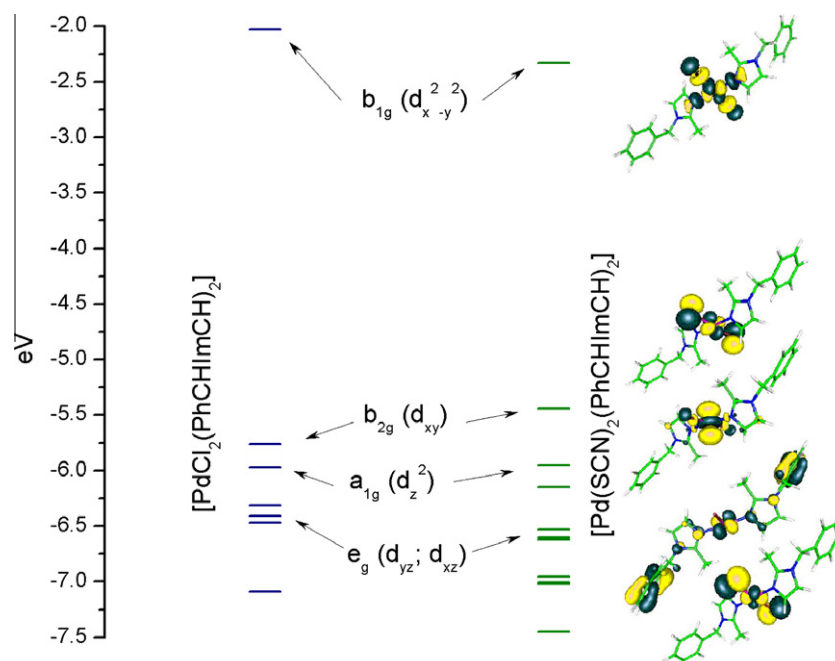


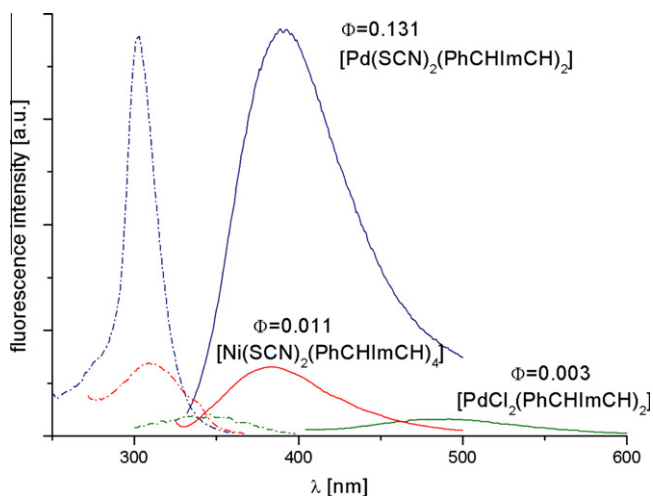
Fig. 4. Splitting of 4d palladium(II) orbital diagram for the **(1)** and **(2)** complexes.

Table 4

The calculated electronic transitions and its assignments to the experimental absorption bands for palladium complexes (1) and (2).

The most important orbital excitations	Character	λ (nm)	f	Exp. λ (nm)
(1)				
H-1 \rightarrow LUMO (97%)	$a_{1g} \rightarrow b_{1g}$	390.1	0.0038	401.5
H-10 \rightarrow LUMO (94%)	$\pi_L \rightarrow b_{1g}$	328.4	0.0204	
H-5 \rightarrow LUMO (87%)	$\pi_{L/Cl} \rightarrow b_{1g}$	321.2	0.0013	
H-11 \rightarrow LUMO (91%)	$\pi_L \rightarrow b_{1g}$	316.7	0.0028	
H-7 \rightarrow LUMO (97%)	$\pi_{L/Cl} \rightarrow b_{1g}$	308.2	0.0002	
H-14 \rightarrow LUMO (17%), H-12 \rightarrow LUMO (79%)	$\pi_L/d_{pd} \rightarrow b_{1g}$	270.9	0.1422	276.1
H-14 \rightarrow LUMO (80%), H-12 \rightarrow LUMO (15%)	$\pi_L/d_{pd} \rightarrow b_{1g}$	236.7	0.3705	
H-1 \rightarrow L + 2 (32%), HOMO \rightarrow L + 1 (41%)	$a_{1g} \rightarrow \pi^*_L; b_{2g} \rightarrow \pi^*_L$	220.9	0.0559	228.4
H-1 \rightarrow L + 4 (41%), HOMO \rightarrow L + 3 (49%)	$a_{1g} \rightarrow \pi^*_L; b_{2g} \rightarrow \pi^*_L$	217.2	0.0149	
H-2 \rightarrow L + 3 (30%), H-2 \rightarrow L + 5 (66%)	$\pi_{L/Cl} \rightarrow \pi^*_L$	211.9	0.0201	211.5
(2)				
H-9 \rightarrow LUMO (10%), H-3 \rightarrow LUMO (48%), H-1 \rightarrow LUMO (37%)	$\pi_L \rightarrow b_{1g}; e_g \rightarrow b_{1g}; \pi_{SCN} \rightarrow b_{1g}$	393.2	0.0063	400.1
H-9 \rightarrow LUMO (51%), H-8 \rightarrow LUMO (41%)	$\pi_L \rightarrow b_{1g}$	328.9	0.0236	325.6
H-9 \rightarrow LUMO (26%), H-8 \rightarrow LUMO (56%), H-4 \rightarrow LUMO (12%)	$\pi_L \rightarrow b_{1g}; e_g \rightarrow b_{1g}$	323.2	0.5346	
H-4 \rightarrow LUMO (20%), H-3 \rightarrow LUMO (24%), H-1 \rightarrow LUMO (49%)	$e_g \rightarrow b_{1g}; \pi_{SCN} \rightarrow b_{1g}$	294.3	0.3616	
H-8 \rightarrow LUMO (53%), H-6 \rightarrow LUMO (18%), H-4 \rightarrow LUMO (22%)	$\pi_L \rightarrow b_{1g}; e_g \rightarrow b_{1g}$	280.4	0.3226	
H-12 \rightarrow LUMO (99%)	$a_{1g} \rightarrow b_{1g}$	265.7	0.0056	264.6
H-12 \rightarrow LUMO (11%), H-8 \rightarrow LUMO (17%), H-4 \rightarrow LUMO (47%), H-1 \rightarrow LUMO (13%)	$a_{1g} \rightarrow b_{1g}; \pi_L \rightarrow b_{1g}; e_g \rightarrow b_{1g}; \pi_{SCN} \rightarrow b_{1g}$	229.3	0.0117	232.5
H-12 \rightarrow LUMO (82%)	$a_{1g} \rightarrow b_{1g}$	214.7	0.0118	

L denotes 1-benzyl-2-methylimidazole.

**Fig. 5.** Excitation and fluorescence spectra of (1), (2) and (3) solutions complex in methanol.

of the complex. On the other hand in the case of complex (3) the nickel d orbitals participate in a lesser degree, in comparison with palladium, in the molecular orbitals engaged in excitation–emission processes. Therefore the difference in the symmetry of the palladium and nickel complexes (2) and (3) square planar and octahedral and different splitting of d orbitals as well as a larger nephelauxetic effect in the 4d than 3d orbitals result in large contribution of d_{pd} in luminescence. In the excitations in palladium complexes the b_{1g} term is engaged which is localized on whole molecule with significant contribution of palladium $d_{x^2-y^2}$ (43%) orbital (SCN^- (39%), $PhCHImCH$ (18%)). In the case of nickel complex (3) excited states are localized on 1-benzyl-2-methylimidazole ligands (100%).

Acknowledgements

The GAUSSIAN09 calculations were carried out in the Wrocław Centre for Networking and Supercomputing, WCSS, Wrocław, Poland, <http://www.wcss.wroc.pl>.

Appendix A. Supplementary material

CCDC 882436, CCDC 883502 and CCDC 885047 contain the supplementary crystallographic data for $[PdCl_2(PhCHImCH)_2]$ (1), $[Pd(SCN)_2(PhCHImCH)_2]$ (2) and $[Ni(NCS)_2(PhCHImCH)_4] \cdot CH_3OH$ (3) complexes. These data can be obtained free of charge via <http://www.ccdc.cam.ac.uk/conts/retrieving.html>, or from the Cambridge Crystallographic Data Centre, 12 Union Road, Cambridge CB2 1EZ, UK; fax: +44 1223 336 033; or e-mail: deposit@ccdc.cam.ac.uk.

References

- [1] D. Kovala-Demertzi, M.A. Demertzi, E. Filiou, A.A. Pantazaki, P.N. Yadav, J.R. Miller, Y. Zheng, D.A. Kyriakidis, *Biometals* 16 (2003) 411.
- [2] E. Budzisz, U. Krajewska, M. Rozalski, A. Szulawska, M. Czyż, B. Nawrot, *Eur. J. Pharmacol.* 502 (2004) 59.
- [3] J. Kuduk-Jaworska, A. Puszko, M. Kibiak, M. Pelczynska, *J. Inorg. Biochem.* 98 (2004) 1447.
- [4] E. Budzisz, M. Miernicka, I-P. Lorenz, P. Mayer, U. Krajewska, M. Rozalki, *Polyhedron* 28 (2009) 637.
- [5] Y. Najajreh, J.M. Perez, C. Navarro-Ranninger, D. Gibson, *J. Med. Chem.* 45 (2002) 5189.
- [6] E. Khazanov, Y. Barenholtz, D. Gibson, Y. Najajreh, *J. Med. Chem.* 45 (2002) 5196.
- [7] N. Andrade-Lopez, J.G. Alvarado-Rodriguez, S. Gonzalez-Montiel, M.G. Rodriguez-Mendez, M.E. Paez-Hernandez, C.A. Galan-Vidal, *Polyhedron* 26 (2007) 4825.
- [8] S.O. Ojwach, I.A. Guzei, J. Darkwa, S.F. Mapolie, *Polyhedron* 26 (2007) 851.
- [9] H. Liang, J. Liu, X. Li, Y. Li, *Polyhedron* 23 (2004) 1619.
- [10] N.A. Piro, J.S. Owen, J.E. Bercaw, *Polyhedron* 23 (2004) 2797.
- [11] R. Chen, J. Bacsá, S.F. Mapolie, *Polyhedron* 22 (2003) 2855.
- [12] L. Ma, R.C. Smith, J.D. Protasiewicz, *Inorg. Chim. Acta* 358 (2005) 3478.
- [13] E. Guney, V.T. Yilmaz, C. Kazak, *Polyhedron* 29 (2010) 1285.
- [14] V. Anbalagan, T.S. Srivastava, *Polyhedron* 23 (2004) 3173.
- [15] J.G. Maleski, P. Zwoliński, *Polyhedron* 39 (2012) 85.
- [16] J.G. Maleski, A. Maroń, *Transition Met. Chem.* 36 (2011) 297.
- [17] C.A. Parker, T.A. Joyce, *Trans. Faraday Soc.* 62 (1966) 2785.
- [18] GAUSSIAN09, Revision A.1, M.J. Frisch, G.W. Trucks, H.B. Schlegel, G.E. Scuseria, M.A. Robb, J.R. Cheeseman, G. Scalmani, V. Barone, B. Mennucci, G.A. Petersson, H. Nakatsuji, M. Caricato, X. Li, H.P. Hratchian, A.F. Izmaylov, J. Bloino, G. Zheng, J.L. Sonnenberg, M. Hada, M. Ehara, K. Toyota, R. Fukuda, J. Hasegawa, M. Ishida, T. Nakajima, Y. Honda, O. Kitao, H. Nakai, T. Vreven, J.A. Montgomery, Jr., J.E. Peralta, F. Ogliaro, M. Bearpark, J.J. Heyd, E. Brothers, K.N. Kudin, V.N. Staroverov, R. Kobayashi, J. Normand, K. Raghavachari, A. Rendell, J.C. Burant, S.S. Iyengar, J. Tomasi, M. Cossi, N. Rega, J.M. Millam, M. Klene, J.E. Knox, J.B. Cross, V. Bakken, C. Adamo, J. Jaramillo, R. Gomperts, R.E. Stratmann, O. Yazyev, A.J. Austin, R. Cammi, C. Pomelli, J.W. Ochterski, R.L. Martin, K. Morokuma, V.G. Zakrzewski, G.A. Voth, P. Salvador, J.J. Dannenberg, S. Dapprich, A.D. Daniels, O. Farkas, J.B. Foresman, J.V. Ortiz, J. Cioslowski, D.J. Fox, GAUSSIAN, Inc., Wallingford CT, 2009.
- [19] A.D. Becke, *J. Chem. Phys.* 98 (1993) 5648.
- [20] C. Lee, W. Yang, R.G. Parr, *Phys. Rev. B* 37 (1988) 785.

- [21] N. Godbout, D.R. Salahub, J. Andzelm, E. Wimmer, *Can. J. Chem.* 70 (1992) 560.
- [22] M.E. Casida, in: J.M. Seminario (Ed.), *Recent Developments and Applications of Modern Density Functional Theory, Theoretical and Computational Chemistry*, vol. 4, Elsevier, Amsterdam, 1996, p. 391.
- [23] E.D. Glendening, A.E. Reed, J.E. Carpenter, F. Weinhold, NBO, version 3.1.
- [24] N.M. O'Boyle, A.L. Tenderholt, K.M. Langner, *J. Comput. Chem.* 29 (2008) 839.
- [25] O.V. Dolomanov, L.J. Bourhis, R.J. Gildea, J.A.K. Howard, H. Puschmann, *J. Appl. Crystallogr.* 42 (2009) 339.
- [26] G.M. Sheldrick, *Acta Crystallogr., Sect. A* A64 (2008) 112.
- [27] T. Ruther, M.C. Done, K.J. Cavell, E.J. Peacock, B.W. Skelton, A. White, *Organometallics* 20 (2001) 5522.
- [28] G.R. Desiraju, T. Steiner, *The Weak Hydrogen Bond in Structural Chemistry and Biology*, Oxford University Press, 1999.